Assessing the Observability of Higher-Order Modes and their Impact on the Localization of Gravitational Wave Sources

Zoe Rosenberg,[1,2,*] Patricia Schmidt,[2,†] and Geraint Pratten[2,‡]

[1] *Department of Physics and Astronomy, Rutgers University, New Brunswick, New Jersey*
[2] *School of Physics and Astronomy and Institute for Gravitational Wave Astronomy, University of Birmingham, Edgbaston, Birmingham, B15 2TT, United Kingdom*

(Dated: August 17, 2023)

Higher order modes are the post-quadrupolar terms of the gravitational radiation multipole expansion, and can have a noticeable effect on waveforms for asymmetric compact binary systems. For a simulated population of 200,000 black hole binary systems, we calculate the signal-to-noise ratios of all modes, (2,|2|) modes, and four selected higher order modes. We perform this calculation for five detector networks, ranging from the fifth observing run (O5) to third-generation detector networks, in order to see how large an impact higher order modes will have in our future gravitational wave observations and how important they are to include in our waveform models. We then consider a selected neutron star-black hole mock signal and perform full Bayesian parameter estimation with varying mode content. Through comparing the source localization of the parameter estimation that included all modes and those that only included one or two modes, we can see how much including higher order modes in parameter estimation improves LIGO skymaps we provide to observational astronomers for electromagnetic follow-ups. We also determine how well including higher order modes in the recovery breaks the degeneracy between the luminosity distance and inclination angle.

I. INTRODUCTION

Gravitational waves (GWs) are perturbations in the fabric of space time. Gravitational radiation is often approximated by the quadrupole formula, but the radiation field can be expanded into a multipole expansion similar to the electromagnetic field. For an in-depth explanation see for example these textbooks [1, 2]. Depending on the parameters of the GW-emitting source, its orientation, and the GW detector sensitivity, it can be crucial to account for higher order terms of this expansion, or higher-order modes, in the waveform templates [3–5]. This is because in order to detect GW signals from compact binaries, matched filtering is used to pick out a signal from the detector noise [6]. Higher order modes are also known as higher spherical harmonics [7] and non-quadrupolar modes. Although the higher order modes are only currently observable in a few percent of binary systems [7], upgraded and next-generation GW detectors will have a much higher rate of detections, and improved sensitivities. As a result, higher order modes will be observable in many more systems. Higher order modes can be used to test general relativity, to break degeneracies such as the inclination of the orbit and the distance to the source [8–10], and to better measure masses and spins.

Taking into account higher order modes is particularly important for asymmetric binary systems, i.e. binaries with very unequal masses and/or unequal spins, and systems with a non-zero inclination of the orbital plane with respect to the observer. This is because higher order modes have a considerable contribution to the observed waveform near the merger for these types of systems. Higher order modes will have their largest contribution for systems with a very large mass ratio, very unequal spins, and those oriented closer to edge-on relative to the GW detectors. An example of this can be seen in Figure 1. Figure 2 then shows a representation of the strains, or signals, of the dominant (quadrupolar) mode, the $(2,|1|)$ higher order mode, and all modes together in relation to the amplitude spectral densities (ASDs) for two selected detectors. In the figure, the signal for all modes and the $(2,|1|)$ mode lie above the ASD curves for the two detector sensitivities in a certain frequency range, meaning those signals should be visible above the detector noise within that frequency range. The signal will look different depending on the parameters of the GW-emitting source. There are the intrinsic parameters, which come from the compact binary system itself, and the extrinsic parameters, which come from the location of the binary system and time of the merger. The primary and secondary masses, spins, and the mass ratio are the intrinsic parameters, and the luminosity distance, right ascension (RA), declination (DEC), inclination angle, polarization angle, and the time of coalescence are the extrinsic parameters.

Physically, higher order modes are small perturbations in the gravitational radiation field. They can be described by the integers (ℓ, m), which are analogous to the quantum numbers (ℓ, m) that can be found in quantum mechanics. The m-modes are split into odd and even. Although both odd and even m modes are excited by asymmetries in the system, asymmetries contribute especially to odd modes.

We will look at the higher order modes in a simulated population of binary black hole systems, which are a type of compact binary coalescences (CBCs). We will then

* zar24@scarletmail.rutgers.edu
† p.schmidt@bham.ac.uk
‡ g.pratten@bham.ac.uk

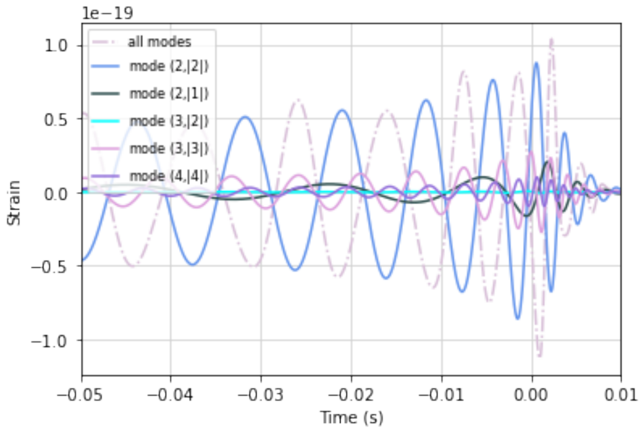

FIG. 1. The time-domain strain $h(t) = h_+(t) \cdot F_+ + h_\times(t) \cdot F_\times$ of a simulated black hole binary system over time. h_+ and $h_\times$ are the plus and cross polarizations of the strain, multiplied with their corresponding antenna response functions. The merger itself occurs where time is equal to zero. The waveform with all modes is plotted, which is what would actually be observed, along with individual modes to show their contribution to the signal near the merger. Since the dominant mode is the (2,|2|) mode, the "all modes" case and (2,|2|) case usually line up very close to (or overlapping with) one another. However, for systems in which higher order modes are prominent, the modes higher than the (2,|2|) mode have a noticeable impact on the total strain. In this extreme case, we have a mass ratio of about 1:7 and an inclination of $\pi/4$. For a system this asymmetric, the "all mode" case varies greatly from the (2,|2|) case, and using the quadrupole approximation on the system would not yield anything close to the correct waveform.

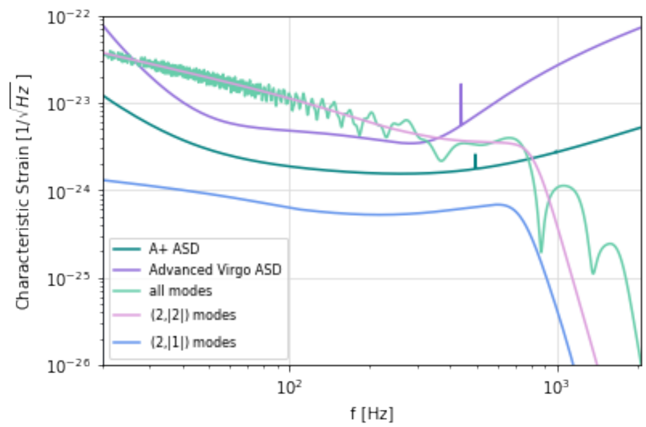

FIG. 2. Amplitude spectral densities (ASDs), which are the square roots of the corresponding power spectral densities (PSDs) for A+ and Advanced Virgo design sensitivities taken from https://dcc.ligo.org/LIGO-T1500293/public. Plotted on the same axes is the characteristic strain of a simulated, in which the absolute value of the frequency-domain strain is multiplied by the square root of the frequency. This multiplication must occur to represent the strain (referred to as the characteristic strain after the multiplication) meaningfully on the same plot. The SNR can be thought of as the area between the characteristic strain and the ASD curve. The individual modes have very smooth characteristic strains, but when higher order modes are accounted for, the strain is very oscillatory and can either increase or reduce the SNR slightly compared to the (2,|2|) mode's characteristic strain.

compute the signal-to-noise ratios (SNRs) of the signals from all modes along with the individual modes of these systems to assess how observable higher-order modes are for different networks of detectors. We will observe which higher order modes have large contributions to the SNRs, which will tell us how important it will be to take higher-order modes into consideration when creating waveform models to be used for future detector networks.

Additionally, we will be conducting parameter estimation for a single neutron star-black hole (NSBH) mock signal (injection). We will complete three different versions of the parameter estimation, in which all of the modes are present in the injection but varying the mode content in the recovery. This is in order to assess how much including higher order modes will improve the source localization, by seeing how well right ascension (RA) and declination (DEC) are constrained in the different cases. It will also show us how well including higher order modes breaks the degeneracy between luminosity distance and inclination angle.

II. RESEARCH METHODS

We make use of the `PyCBC` [11], `LALSuite` [12], and parallel `bilby` [13] Python packages for this research, in addition to `numpy` [14], `scipy` [15], and `pandas` [16, 17].

A. Input parameters

We generated a black hole binary population of $200,000$ unique systems. This population draws from our knowledge of binary black hole (BBH) distributions after the third observing run (O3) for the primary and secondary black hole masses, the mass ratio, the spin magnitudes [18] as shown in Figure 3. The luminosity distances from Earth are determined by distributing the black holes according to the measured merger rate following a power law with power law index of 2.9. The spin tilt angles, which are the angles between the orbital angular momentum of the system and the individual spins are given in spherical coordinates, which we convert into Cartesian coordinates, so that their values are compatible with the `lalsimulation` waveform generator [12], and are drawn from isotropic distributions. The masses are initially drawn from a distribution (Figure 3) that is not redshifted, i.e. in the source-frame. Since gravitational waves travel at the speed of light, they experience redshift just like electromagnetic waves. Due to this redshift, the masses we observe in GW detectors are different to the actual physical masses [8–10]. Using the luminosity distances converted to redshifts, we converted the physical masses to redshifted or detector-frame masses to use in the waveform generator. In order to convert from the luminosity distance to the redshift, we assume cosmological parameters from Planck15 [19].

The the cosine of the inclination angle and the polarization, right ascension, and declination angles for the population are all drawn from uniform distributions. The inclination angle is defined as the angle between the orbital angular momentum of the system and the light-of-sight at the reference frequency. The polarization angle is the angle which measures how much of the signal is in the plus polarization and how much is in the cross polarization, and right ascension and declination define where the system is in the night sky. Inclination angles, polarization angles, and declination angles are between zero and π, and right ascensions are between zero and 2π. The time of coalescence t_c, or GPS time, was chosen to be some arbitrary value, as it does not change the output of the code.

B. Population signal-to-noise ratios

In order to compute the SNRs ρ, we generated the strain for each binary in our population, where the frequency-domain strain $\tilde{h}^D_S(f)$ in a detector D is:

$$\tilde{h}^D_S(f) = \tilde{h}_+(f) \cdot F_+ + \tilde{h}_\times(f) \cdot F_\times \tag{1}$$

using `lalsimulation` [12] and the waveform model `IMRPhenomXPHM` [20–22]. The plus and cross polarizations are $\tilde{h}_+(f)$ and $\tilde{h}_\times(f)$, respectively. The functions F_+ and $F_\times$ are antenna response functions, which take into account that gravitational wave detectors are not equally sensitive to gravitational waves from every direction. The waveform model `IMRPhenomXPHM` [20–22] accounts for both higher-order modes and precession. Precession occurs when the individual black holes spins are misaligned with the orbital angular momentum of the system. We then calculate SNRs using `PyCBC` [11] for several different modes for all of the binary systems. For each system, SNRs for all modes together, and the (2,|2|), (3,|3|), (4,|4|), (2,|1|), and (3,|2|) modes are individually generated. We compute the optimal SNR, in which for data d with noise n and signal s, assumes that there is no noise and the signal is known (and is equal to the injected one). In equation form, $d = n + s = 0 + h$ so

$$\rho^2_D = 4Re\int_{f_{min}}^{f_{max}} \frac{\tilde{h}^D_S \cdot \tilde{h}^{D*}_S}{S^D_N(f)} df \tag{2}$$

Although we know the signal exactly and it matches the strain, the gravitational wave detectors are not equally sensitive at all frequencies, which can be seen from the power spectral density (PSD) as shown in Figure 4. In Equation (2), the PSD is denoted by $S^D_n(f)$ and is the denominator inside the integral, acting as a normalization factor. The PSD curve is also sometimes called a "noise" curve, and the GW signal can only be detected by the detector when it falls above said curve (as in Figure 2). As can be seen, GW detectors are only able to detect signals that span a certain frequency range. For the current generation, this range is from around 20 Hz to about 2 kHz, or from around $1M_\odot$ to a few hundred solar masses. The PSDs for all detectors that we used can be seen in Figure 4.

We calculate the SNR using `PyCBC` [11], which implements (2) and takes care of any relevant data conditioning. We then calculate the network SNR, which is the quadrature sum of each individual detector SNR. This is a helpful quantity to know because it is the maximum SNR observable by the detector network when using the optimal SNR. As the current threshold for GW SNRs in a single detector is around 4-6, we look into systems for which the network SNR is greater than a threshold of 8.

We used five different detector networks to calculate the network SNR. According to their sensitivity (from lowest to highest): The first network is composed of A+ LIGO Hanford and Livingston, and Advanced Virgo. The second is then A+ LIGO Hanford, Voyager LIGO Livingston, and Advanced Virgo. The third is composed of Voyager LIGO Hanford and Livingston and Advanced Virgo. The fourth is Voyager LIGO Hanford, Cosmic Explorer (CE) LIGO Livingston, and Einstein Telescope (ET) Virgo. Finally, the most sensitive network uses CE for LIGO Hanford and Livingston and ET for Virgo. Our networks are summarized in Table I.

TABLE I. Detector Networks

	H	L	V
1	A+	A+	adV
2	A+	Voy	adV
3	Voy	Voy	adV
4	Voy	CE	ET
5	CE	CE	ET

C. Parameter estimation

Much of GW astrophysics relies on Bayesian statistics, as it is a powerful tool in parameter estimation. Bayes' theorem states

$$p(\theta|d) = \frac{\mathcal{L}(d|\theta)\pi(\theta)}{\mathcal{Z}} \tag{3}$$

where $p(\theta|d)$ is the posterior distribution, θ is the set of parameters we are trying to estimate, $\mathcal{L}(d|\theta)$ is the

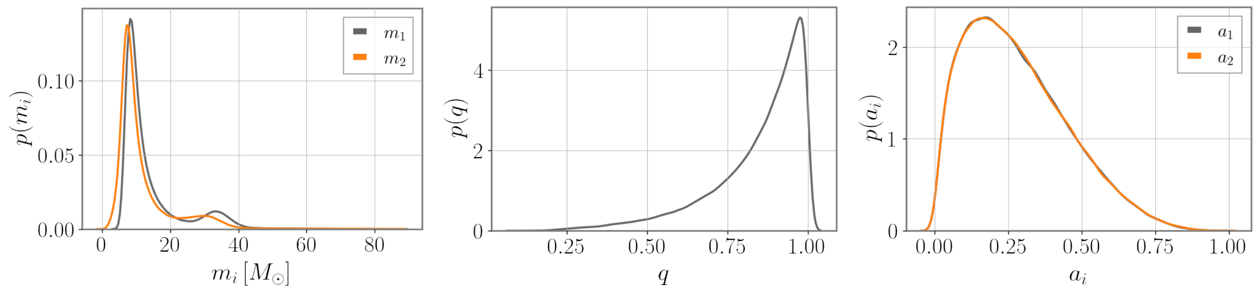

FIG. 3. Source-frame component mass (left), mass ratio (center), and spin magnitude (right) distributions from the generated population of 200,000. Based off knowledge of the distributions for BBH population intrinsic parameters after O3 [18].

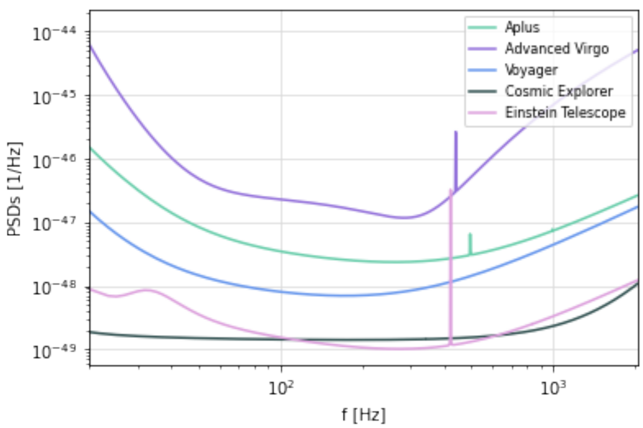

FIG. 4. The different power spectral densities (PSDs) which we use the for different detector networks considered in this project. Aplus and Advanced Virgo will be in operation by O5, Cosmic Explorer and the Einstein Telescope are third-generation detectors, and Voyager falls in-between.

likelihood function, $\pi(\theta)$ is the prior distribution, and $\mathcal{Z}$ is the normalization factor [23]. The normalization factor is called the evidence, which written mathematically is

$$\mathcal{Z} \equiv \int d\theta \mathcal{L}(d|\theta)\pi(\theta) \tag{4}$$

and is formally a likelihood function [23]. For this work, θ (or in this case, $\vec{\theta}$) consists of all the intrinsic and extrinsic parameters of the NSBH system. We are especially interested in the parameters RA and DEC, which will tell us how well the source is localized, and luminosity distance d_L and inclination angle θ_{jn}, which will show us how well the degeneracy between the two is broken, depending on which higher modes were present in the waveform model used for the recovery.

We use two parallel jobs with parallel `bilby` [13] and the `dynesty` sampler [24] in order to sample the posterior distributions. `dynesty` uses a type of Nested Sampling, which estimates $\mathcal{Z}$, or the evidence, for a particular $\vec{\theta}$. As the code runs, there are virtual "particles" known as walkers that move in a random walk through the parameter space to higher and higher likelihoods. The code runs until a certain convergence criteria is met, and the variables in $\vec{\theta}$ are well-constrained. In this case the convergence criteria is $d \log \mathcal{Z} = 0.1$, so when the change in the log of the evidence is less than 0.1, the job will complete and merge the two parallel pieces. The `dynesty` sampler specifically uses Dynamic Nested Sampling, which is described in detail in [24].

We use Gaussian noise and chose an arbitrary GPS time with a sampling frequency of 4096 Hz and a minimum frequency of 20 Hz. The injection is composed of a non-spinning neutron star and a black hole with a spin that is anti-aligned with the orbital angular momentum. The injection also has a mass ratio of about 1:3, which is consistent with NSBHs we have observed to date [25]. All of the parameters for the injection were chosen so that if the signal were real, it would likely produce an electromagnetic counterpart (depening on the nuclear equation of state of the neutron star, which we neglect here). The luminosity distance was chosen to be 250 Mpc in order to be in range of ground-based optical telescopes such as the Rubin Observatory [26], and the distance was marginalized to help with computational speed. The inclination angle was set to about 30 degrees so that if the system were to disrupt and create a short gamma-ray burst, it would be within the detectable range in inclination angles. Table II lists all of the chosen parameter values and the optimal network SNR for the injection (using the LIGO Hanford, LIGO Livingston, and Virgo network).

We inject the same parameters and waveform model (`IMRPhenomXPHM` [20–22]) for three different parameter estimations with changes to the mode content used in the recovery for each. One is set to recover the signal using all modes, one only for the (2,|2|) modes, and one for both the (2,|2|) and the (2,|1|) modes. For the recovery using (2,|2|) modes only, we used the waveform model `IMRPhenomXP` [20, 21], and for the other two runs, we used the model `IMRPhenomXPHM` [20–22].

TABLE II. Injection Parameter Values

Parameter	Value	Units
m_1	5.8	$[M_\odot]$
m_2	1.35	$[M_\odot]$
d_L	250	[Mpc]
θ_{jn}	0.417	[rad]
ψ	1.17	[rad]
phase	5.8	[rad]
RA	3.3	[rad]
DEC	0.5	[rad]
a_1	0.7	
a_2	0.0	
ϕ_{12}	1.21	[rad]
ϕ_{jn}	2.02	[rad]
SNR	45.62	

III. RESULTS

A. Population signal-to-noise ratios

For the least sensitive network (see Table I), 28,785 samples out of the 200,000 sample size had a network signal-to-noise (SNR) ratio greater than 8. For our most sensitive network, 197,794 samples out of 200,000 had SNRs > 8. Since the number of signals that make the SNR cutoff increases so drastically over the improving detector networks, we expect the number of systems with observable contributions from higher order modes to drastically increase as well.

In Figure 5, we represent these SNRs using the inverse cumulative distribution function (CDF). All modes, only the (2,|2|) modes, and individual higher order modes are each plotted on separate graphs. Each graph starts off the same, as 100 percent of the BBH systems have an SNR>0. However, when increasing the SNR, we observe differences between the graphs. The (2,|2|) mode graph looks almost identical to the graph for all modes, which is to be expected since it is the dominant mode. The even m modes, or specifically the (3,|2|) and (4,|4|) modes, also have a similar shape to the graph for all modes. The odd m modes, or specifically the (2,|1|) and (3,|3|) modes, tend to have a flatter slope for their 1-CDF curves. This shows that as the SNRs of each of those modes increases, the percentage of BBH systems that have SNRs greater than that value decreases more slowly than in the other cases. In other words, a higher percentage of BBH systems will have larger SNRs for the (2,|1|) and (3,|3|) modes, especially as network sensitivity increases. Since the odd m modes are affected more strongly by asymmetries than even m modes, this result makes physical sense.

B. Parameter estimation

We found that for the parameter estimation which recovers all modes, the source was extremely well-localized. This can be seen in Figure 6 in how the 50 percent confidence region spans only two square degrees, and how the 90 percent confidence region spans only 6 square degrees. We recover the inclination angle and luminosity distance with good accuracy, with values of $\theta_{jn} = 0.45^{+0.10}_{-0.08}$ and $d_L = 243.09^{+8.37}_{-9.96}$. The true values of the luminosity distance and the inclination angle both fall within their respective ranges of uncertainty.

For the parameter estimation which recovers the (2,|2|) and the (2,|1|) modes, we observe almost the exact same skymap as the case which recovers all modes (seen in the middle left-hand plot of Figure 6. As this case excludes every other higher order mode in the recovery, the source is surprisingly well-localized for such a simplification. The inclination angle and luminosity distance are recovered less accurately than the case with all modes in the recovery, but still do a decent job of estimating their values. The inclination angle is recovered to be $\theta_{jn} = 0.24^{+0.13}_{-0.05}$, and the luminosity distance is $d_L = 235.83^{+9.61}_{-9.03}$. Although both of the true values fall outside their respective ranges of uncertainty, neither of them fall very far outside.

For the case which recovers only the (2,|2|) mode, we also see the same sky localization as our other cases. This may be a result of the specific injection we chose for this work. The inclination angle and luminosity distance are $\theta_{jn} = 0.31^{+0.18}_{-0.09}$ and $d_L = 238.49^{+9.02}_{-10.35}$, respectively. They are recovered to be closer to their actual injected values than the case that also includes the (2,|1|) mode, but the ranges of uncertainty for both parameters are slightly larger (see Figure 6). We would expect the inclination angle and luminosity distance values to be further from their actual values in this case than in the case which also includes the (2,|1|) modes, but as expected, the degeneracy in this case is more obvious than in the case that also includes the (2,|1|) modes (as seen in Figure 6).

IV. DISCUSSION

Looking at Figure 5 we can see that with more sensitive detector networks, the percentage of BBH systems with higher SNRs increases. With SNRs in past and current observing runs tending to be mostly around 8 and reaching a maximum around 30, we can see that there will be a drastic upwards shift in the SNRs we will be able to observe. Therefore, for the BBH signals with higher SNRs, the part of the SNR that comes from higher order modes will go from being a small percent of a small value to a small percent of a large value. Since detection rates will also be much higher for future detectors, we will observe signals with noticeable higher order mode contributions to the SNR more frequently (especially for odd m modes).

In our differing parameter estimation runs, we saw that the source localization was seemingly unaffected by the inclusion of higher-order modes. This is an unexpected result, because we predicted the sky localization would improve with the inclusion of more higher-order modes for an injection with such asymmetric masses and a non-zero inclination angle. However, this is only using one injection, and is by no means an in-depth investigation into source localization with higher-order modes. We still expect the inclusion of higher-order modes in the recovery of parameter estimation to improve the skymaps of other injections which have sizable strain contributions from higher-order modes, and the area needs further investigation. Performing a similar parameter estimation study for a larger number of systems that would have potential observable electromagnetic counterparts would give us a much better idea of how much including higher-order modes may improve source localization. The degeneracy between the luminosity distance and the inclination angle was broken by including all modes in the recovery, and wasn't too large of a problem when just accounting for the $(2, |2|)$ and $(2, |1|)$ modes in the recovery. When only the $(2, |2|)$ mode was accounted for in the recovery, the degeneracy was much more visible in the corner plot (see Figure 6). However, using this injection, the inclination angle and distance were actually recovered better using only the $(2, |2|)$ mode in the recovery than both the $(2, |2|)$ and $(2, |1|)$ modes. This is also something that could be expanded upon in future work, by studying the result of parameter estimations for more injections.

Taking higher order modes into account is going to continue increasing in importance as we increase our global network sensitivity for detecting gravitational waves. We conclude that higher order modes, especially the $(2,|1|)$ and $(3,|3|)$ modes, will have a sizable contribution to the SNRs of our future GW observations. Accounting for higher order modes in parameter estimation could potentially improve the source localization of future events, but this needs further investigation. If further studies show that higher-order modes can greatly improve source localization, it may be worth considering implementing higher-order modes into low-latency parameter estimation runs. Considering higher order modes also has the capability of breaking the luminosity distance-inclination angle degeneracy, allowing us to constrain both values accurately and therefore learn a lot more about the system.

ACKNOWLEDGEMENTS

Thanks to Dr. Patricia Schmidt for her mentorship and her many helpful explanations. Thanks to the University of Birmingham Institute for Gravitational Wave Astronomy for hosting me, and to the doctoral students for welcoming me and answering my countless questions (especially Natalie, Lucy, and Alice).

Thanks to the UFL IREU team: Dr. Paul Fulda, Dr. Peter Wass, Dr. Nathaniel Strauss, and Dr. Kathryn McGill, for all of their hard work in making this opportunity possible. Finally, thanks to my IREU peers for their inspiration and camaraderie. This work was made possible with National Science Foundation funding (NSF PHY-1950830).

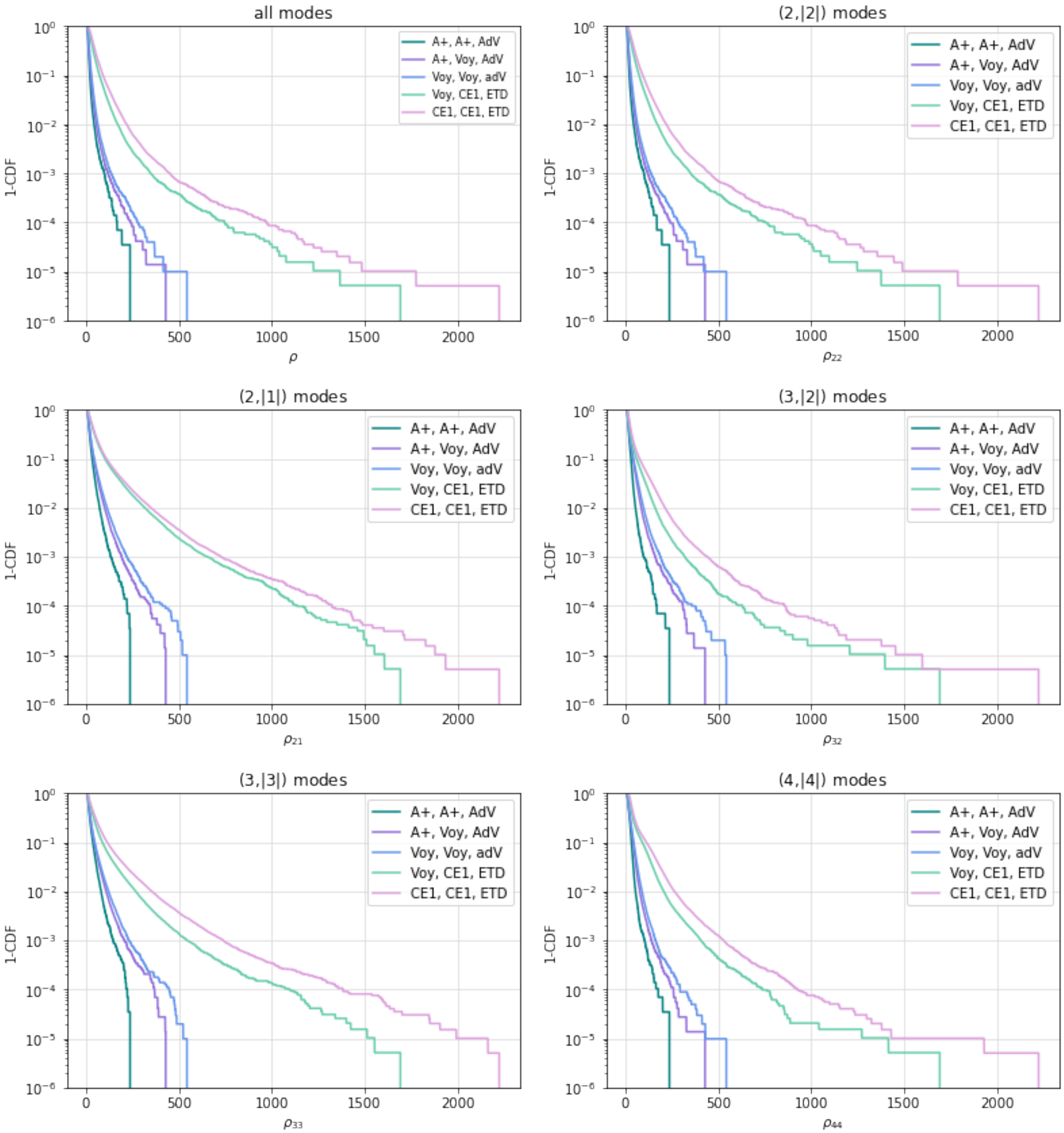

FIG. 5. Cumulative distribution functions for each detector network, organized by mode content. Each curve begins such that all of the systems have SNRS>0, but split according to sensitivity as SNRs increase (with the more sensitive networks reaching larger SNRs, and having higher percentages of BBH signals with higher SNRs).

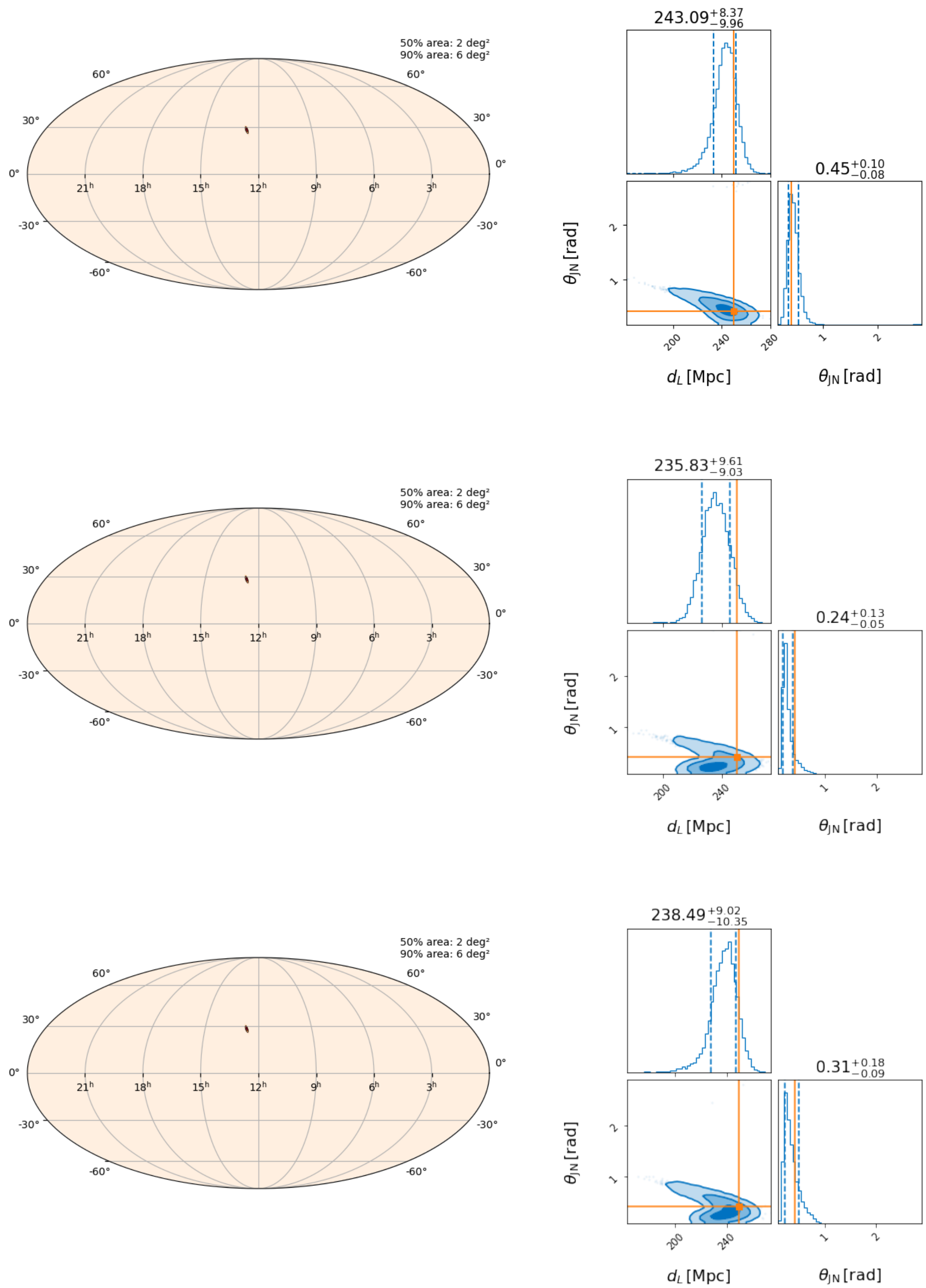

FIG. 6. The left-hand plots show the source localization of the signal on a projection of the sky, and the right-hand plots show the distance-inclination degeneracy for the three cases: all modes (top), (2, |2|) and (2, |1|) modes (middle), and (2, |2|) modes only (bottom). The degeneracy between inclination angle and luminosity distance, which can be seen by the blue region in the corner plot appearing more banana- or boomerang-shaped, is gradually improved with the inclusion of the (2, |1|) mode, and then all modes, in the recovery of the parameter estimation.

[1] M. Maggiore, *Gravitational Waves. Vol. 1: Theory and Experiments* (Oxford University Press, 2007).

[2] M. Maggiore, *Gravitational Waves. Vol. 2: Astrophysics and Cosmology* (Oxford University Press, 2018).

[3] I. Harry, J. C. Bustillo, and A. Nitz, Searching for the full symphony of black hole binary mergers, Phys. Rev. D **97**, 023004 (2018).

[4] J. Calderón Bustillo, S. Husa, A. M. Sintes, and M. Pürrer, Impact of gravitational radiation higher order modes on single aligned-spin gravitational wave searches for binary black holes, Phys. Rev. D **93**, 084019 (2016).

[5] J. Calderón Bustillo, P. Laguna, and D. Shoemaker, Detectability of gravitational waves from binary black holes: Impact of precession and higher modes, Phys. Rev. D **95**, 104038 (2017).

[6] B. Allen, W. G. Anderson, P. R. Brady, D. A. Brown, and J. D. E. Creighton, FINDCHIRP: An Algorithm for detection of gravitational waves from inspiraling compact binaries, Phys. Rev. D **85**, 122006 (2012), arXiv:gr-qc/0509116.

[7] C. Mills and S. Fairhurst, Measuring gravitational-wave higher-order multipoles, Physical Review D **103**, 10.1103/physrevd.103.024042 (2021).

[8] D. Marković, Possibility of determining cosmological parameters from measurements of gravitational waves emitted by coalescing, compact binaries, Phys. Rev. D **48**, 4738 (1993).

[9] S. Nissanke, D. E. Holz, S. A. Hughes, N. Dalal, and J. L. Sievers, EXPLORING SHORT GAMMA-RAY BURSTS AS GRAVITATIONAL-WAVE STANDARD SIRENS, The Astrophysical Journal **725**, 496 (2010).

[10] P. B. Graff, A. Buonanno, and B. Sathyaprakash, Missing link: Bayesian detection and measurement of intermediate-mass black-hole binaries, Physical Review D **92**, 10.1103/physrevd.92.022002 (2015).

[11] A. Nitz, I. Harry, D. Brown, C. M. Biwer, J. Willis, T. D. Canton, C. Capano, T. Dent, L. Pekowsky, S. De, M. Cabero, G. S. C. Davies, A. R. Williamson, D. Macleod, B. Machenschalk, F. Pannarale, P. Kumar, S. Reyes, dfinstad, S. Kumar, S. Wu, M. Tápai, L. Singer, veronica villa, S. Khan, S. Fairhurst, K. Chandra, A. Nielsen, S. Singh, and T. Massinger, gwastro/pycbc: v2.1.2 release of pycbc (2023).

[12] LIGO Scientific Collaboration, LIGO Algorithm Library - LALSuite, free software (GPL) (2018).

[13] R. J. E. Smith, G. Ashton, A. Vajpeyi, and C. Talbot, Massively parallel Bayesian inference for transient gravitational-wave astronomy, **498**, 4492 (2020), arXiv:1909.11873 [gr-qc].

[14] C. R. Harris, K. J. Millman, S. J. van der Walt, R. Gommers, P. Virtanen, D. Cournapeau, E. Wieser, J. Taylor, S. Berg, N. J. Smith, R. Kern, M. Picus, S. Hoyer, M. H. van Kerkwijk, M. Brett, A. Haldane, J. F. del Río, M. Wiebe, P. Peterson, P. Gérard-Marchant, K. Sheppard, T. Reddy, W. Weckesser, H. Abbasi, C. Gohlke, and T. E. Oliphant, Array programming with NumPy, Nature **585**, 357 (2020).

[15] P. Virtanen, R. Gommers, T. E. Oliphant, M. Haberland, T. Reddy, D. Cournapeau, E. Burovski, P. Peterson, W. Weckesser, J. Bright, S. J. van der Walt, M. Brett, J. Wilson, K. J. Millman, N. Mayorov, A. R. J. Nelson, E. Jones, R. Kern, E. Larson, C. J. Carey, İ. Polat, Y. Feng, E. W. Moore, J. VanderPlas, D. Laxalde, J. Perktold, R. Cimrman, I. Henriksen, E. A. Quintero, C. R. Harris, A. M. Archibald, A. H. Ribeiro, F. Pedregosa, P. van Mulbregt, and SciPy 1.0 Contributors, SciPy 1.0: Fundamental Algorithms for Scientific Computing in Python, Nature Methods **17**, 261 (2020).

[16] T. pandas development team, pandas-dev/pandas: Pandas (2023), if you use this software, please cite it as below.

[17] Wes McKinney, Data Structures for Statistical Computing in Python, in *Proceedings of the 9th Python in Science Conference*, edited by Stéfan van der Walt and Jarrod Millman (2010) pp. 56 – 61.

[18] R. Abbott *et al.* (KAGRA, VIRGO, LIGO Scientific), Population of Merging Compact Binaries Inferred Using Gravitational Waves through GWTC-3, Phys. Rev. X **13**, 011048 (2023), arXiv:2111.03634 [astro-ph.HE].

[19] P. A. R. Ade *et al.* (Planck), Planck 2015 results. XIII. Cosmological parameters, Astron. Astrophys. **594**, A13 (2016), arXiv:1502.01589 [astro-ph.CO].

[20] G. Pratten *et al.*, Computationally efficient models for the dominant and subdominant harmonic modes of precessing binary black holes, Phys. Rev. D **103**, 104056 (2021), arXiv:2004.06503 [gr-qc].

[21] G. Pratten, S. Husa, C. Garcia-Quiros, M. Colleoni, A. Ramos-Buades, H. Estelles, and R. Jaume, Setting the cornerstone for a family of models for gravitational waves from compact binaries: The dominant harmonic for nonprecessing quasicircular black holes, Phys. Rev. D **102**, 064001 (2020), arXiv:2001.11412 [gr-qc].

[22] C. García-Quirós, M. Colleoni, S. Husa, H. Estellés, G. Pratten, A. Ramos-Buades, M. Mateu-Lucena, and R. Jaume, Multimode frequency-domain model for the gravitational wave signal from nonprecessing black-hole binaries, Phys. Rev. D **102**, 064002 (2020), arXiv:2001.10914 [gr-qc].

[23] E. Thrane and C. Talbot, An introduction to bayesian inference in gravitational-wave astronomy: Parameter estimation, model selection, and hierarchical models, Publications of the Astronomical Society of Australia **36**, 10.1017/pasa.2019.2 (2019).

[24] J. S. Speagle, DYNESTY: a dynamic nested sampling package for estimating Bayesian posteriors and evidences, **493**, 3132 (2020), arXiv:1904.02180 [astro-ph.IM].

[25] R. Abbott *et al.* (LIGO Scientific, VIRGO, KAGRA), GWTC-3: Compact Binary Coalescences Observed by LIGO and Virgo During the Second Part of the Third Observing Run, (2021), arXiv:2111.03606 [gr-qc].

[26] P. S. Cowperthwaite, V. A. Villar, D. M. Scolnic, and E. Berger, LSST Target-of-Opportunity Observations of Gravitational Wave Events: Essential and Efficient, Astrophys. J. **874**, 88 (2019), arXiv:1811.03098 [astro-ph.HE].

[27] B. S. Sathyaprakash and B. F. Schutz, Physics, astrophysics and cosmology with gravitational waves, Living Reviews in Relativity **12**, 10.12942/lrr-2009-2 (2009).